

BROADBAND PHYSICS-BASED MODELING OF MICROWAVE PASSIVE DEVICES THROUGH FREQUENCY MAPPING

John W. Bandler, *Fellow, IEEE*, Mostafa A. Ismail, *Student Member, IEEE* and
José E. Rayas-Sánchez, *Senior Member, IEEE*

Keywords empirical models, modeling, passive devices, frequency mapping, rational functions, neural networks

Abstract We present a new computer-aided modeling methodology to develop physics-based models for passive components. We coherently integrate full-wave EM simulators, artificial neural networks, multivariable rational functions, dimensional analysis and frequency mapping to establish broadband models. We consider both frequency-independent and frequency-dependent empirical models. Frequency mapping is used to develop the frequency-dependent empirical models. Useful properties of the frequency mapping are also presented and utilized in the modeling process. We also consider the transformation from frequency-dependent models into frequency-independent ones. We illustrate the modeling process through various examples, including a microstrip right angle bend, a microstrip via, a microstrip double-step (to be used as a basic element of constructing a coarse model for nonuniform or tapered microstrip transmission lines) and a CPW step junction.

I. INTRODUCTION

We present a new computer-aided modeling methodology to develop physics-based empirical

This work was supported in part by the Natural Sciences and Engineering Research Council of Canada (NSERC) under Grants OGP0007239 and STP0201832, and through the Micronet Network of Centres of Excellence. J.E. Rayas-Sánchez is funded by CONACYT (Consejo Nacional de Ciencia y Tecnología, Mexico), as well as by ITESO (Instituto Tecnológico y de Estudios Superiores de Occidente, Mexico).

J.W. Bandler, M.A. Ismail and J.E. Rayas-Sánchez are with the Simulation Optimization Systems Research Laboratory and the Department of Electrical and Computer Engineering, McMaster University, Hamilton, Ontario, Canada L8S 4K1.

J.W. Bandler is also with Bandler Corporation, P.O. Box 8083, Dundas, Ontario, Canada L9H 5E7.

models (“coarse” models) for microwave passive components. We integrate in a coherent way EM simulators, artificial neural networks (ANN) [1,2], multivariable rational functions (MRF) [3], dimensional analysis [4,5] and frequency mapping [6,7] to establish models valid over broad frequency ranges. We consider frequency-independent empirical models (FIEM) and frequency-dependent empirical models (FDEM). In the FDEM we use the frequency mapping approach [6,7] which implicitly introduces frequency dependency into the model elements. We also exploit the odd property of the frequency mapping, that is the transformed or “coarse” model frequency must be an odd function of frequency. ANNs or MRFs are used to approximate these elements as well as the frequency mapping. MRFs enable us to transform a simple FDEM to an equivalent FIEM. This transformation can be expedited by impedance synthesis [8] as we will see in the examples. Dimensional analysis [4,5] determines the functionality of the model elements and the frequency mapping on the components’ geometrical and physical parameters. It also reduces the amount of training data required in the approximation process. The data required to develop FIEMs or FDEMs is obtained by accurate but time intensive full-wave EM simulators (referred to in the space mapping literature as “fine” models [6]). We illustrate the process through various examples, including a microstrip right angle bend, a microstrip via, a microstrip double-step (to be used as a basic element of constructing a coarse model for nonuniform or tapered microstrip transmission lines) and a CPW step junction.

Equivalent circuits can be obtained from the literature or can be visualized by microwave engineers through their understanding and expertise of microwave components. We believe that, though simple, they have advantages over black-box modeling of microwave components since they embody physical characteristics (at least at low frequencies) of the actual components. A shortcoming is that those equivalent circuits may fail to give good accuracy at high frequencies due to dispersion. We address dispersive effects by introducing the frequency dependency into the elements of the equivalent circuits.

II. FREQUENCY INDEPENDENT EMPIRICAL MODELS (FIEM)

Consider a microwave component modeled by a fine model (typically a suitable full-wave EM simulator) and a coarse model (empirical model) in the form of an equivalent circuit. We assume that the topology of the equivalent circuit is known but the empirical formulas of their elements are to be determined. This concept is shown in Fig. 1, where \mathbf{x}_f is an n -dimensional vector representing the parameters of the microwave component, \mathbf{R}_f is a vector representing the fine model responses (typically the scattering parameters), ω is the frequency and \mathbf{R}_c is a vector representing the coarse model responses. The development of the FIEM is shown in Fig. 2, where \mathbf{y} is an l -dimensional vector representing the empirical formulas of the elements of the coarse model. Applying dimensional analysis [4,5] the vector \mathbf{y} becomes a function of an n_r -dimensional vector \mathbf{x}_r ($n_r < n$), which we call the reduced input parameter vector (we will show in the examples how to construct this vector). Through ANNs [1, 2] or MRFs [3] we approximate \mathbf{y} in a certain region of parameters and frequency as

$$\mathbf{y} \approx \mathbf{Q}(\mathbf{x}_r, \mathbf{w}) \quad (1)$$

where \mathbf{w} is the set of parameters of the ANNs or the MRFs. The set \mathbf{w} is evaluated by solving the optimization problem

$$\min_{\mathbf{w}} \left\| [\mathbf{e}_{11}^T \cdots \mathbf{e}_{1M}^T \mathbf{e}_{21}^T \cdots \mathbf{e}_{2M}^T \cdots \mathbf{e}_{N1}^T \cdots \mathbf{e}_{NM}^T]^T \right\| \quad (2)$$

where $\| \cdot \|$ is a suitable norm, N is the total number of training points, M is the number of frequency points per frequency sweep and \mathbf{e}_{ij} is an error vector given by

$$\mathbf{e}_{ij} = \mathbf{R}_f(\mathbf{x}_{f_i}, \omega_j) - \mathbf{R}_c(\mathbf{Q}(\mathbf{x}_{r_i}, \mathbf{w}), \omega_j) \quad (3)$$

The optimization problem in (2) is solved by the Huber optimizer implemented in OSA90 [13]. The training points are selected according to the Central Composite Design (CCD) [9] and more training points are added if necessary.

III. FREQUENCY DEPENDENT EMPIRICAL MODELS (FDEM)

Two approaches can be used to introduce frequency dependency to the elements of the FDEM. One approach is to make the reduced vector \mathbf{x}_r and hence \mathbf{y} depend on frequency as well as other physical parameters (Fig. 3). The second approach exploits the frequency mapping (transformation) concept [6,7], where we simulate the coarse model at a different frequency from the fine model. We call this frequency the coarse model frequency ω_c . Frequency mappings (transformations) have roots in classical filter design, for example, low-pass to band-pass or high-pass transformations [10]. The development of the FDEM using this approach is shown in Fig. 4. The dependency of ω_c on ω as well as the physical parameters is determined by applying dimensional analysis. Both \mathbf{y} and ω_c can be approximated by an ANN or a MRF as

$$\mathbf{y} \approx \mathbf{Q}(\mathbf{x}_r, \mathbf{w}_1) \quad (4a)$$

$$\omega_c \approx \Omega(\mathbf{x}_r, \omega, \mathbf{w}_2) \quad (4b)$$

where \mathbf{w}_1 and \mathbf{w}_2 are the parameters of the ANN or MRF. These parameters are evaluated by solving an optimization problem similar to (2) with the error vector \mathbf{e}_{ij} given by

$$\mathbf{e}_{ij} = \mathbf{R}_f(\mathbf{x}_{f_i}, \omega_j) - \mathbf{R}_c(\mathbf{Q}(\mathbf{x}_{r_i}, \mathbf{w}_1), \Omega(\mathbf{x}_{r_i}, \omega_j, \mathbf{w}_2)) \quad (5)$$

Properties of the Frequency Mapping

Simulating the coarse model at a different frequency from that of the fine model is an implicit way of introducing frequency dependency to the elements of the coarse model. For example, if the device is lossless the coarse model contains only lossless lumped-elements (lossless inductors and capacitors). In this case, a FDEM simulated at ω_c and with a circuit element vector \mathbf{y} is equivalent to a FDEM simulated at ω and a circuit elements vector \mathbf{y}_1 given by

$$\mathbf{y}_1 = (\omega_c / \omega) \mathbf{y} \quad (6)$$

This can be proved as follows. For any inductor L and capacitor C (simulated at frequency ω_c) in \mathbf{y} we have

$$Z_L = j \omega (L \omega_c / \omega) \quad (7a)$$

$$Y_c = j \omega (C \omega_c / \omega) \quad (7b)$$

Therefore, the circuit elements vector \mathbf{y}_1 (simulated at frequency ω) is related to the vector \mathbf{y} by (6). Furthermore, the coarse model frequency ω_c should be an odd function of ω . This results from the even and odd properties [10] of an arbitrary frequency-dependent impedance $Z(\omega)$, where the real (imaginary) part should be an even (odd) function of frequency. For example, if an inductor L is simulated at frequency ω_c the equivalent impedance $Z_L = j\omega_c L$ is purely imaginary, hence Z_L and consequently ω_c should be an odd function of ω . The odd property is also preserved when using the frequency mapping to transform a low-pass filter into a high- or a band-pass filter [10]. This property is used in conjunction with dimensional analysis to further reduce the number of parameters of the ANN or the MRF approximating ω_c .

Transformation of FDEMs into FIEMs

The advantage of using MRFs to approximate the frequency mapping is that we can transform the FDEM into an equivalent FIEM. This transformation involves one-port impedance synthesis, which states that the impedance we want to realize should be a real rational function [8]. For example, the impedances associated with an inductor L and a capacitor C (simulated at ω_c) in the circuit elements vector \mathbf{y} are $Z_L = j\omega_c L$ and $Z_C = 1/j\omega_c C$, respectively. Those impedances can be realized using any of the one-port impedance synthesis techniques such as the first Foster realization or second Foster realization or ladder realization [8]. In the examples presented here, we notice that the frequency ω_c takes the form

$$\omega_c = \omega \frac{f_1 - \omega^2 f_2}{f_3 - \omega^2 f_4} \quad (8)$$

where f_1, f_2, f_3, f_4 are polynomials of the device physical parameters. Therefore, the impedances associated with an inductor L and a capacitor C in the circuit elements vector \mathbf{y} are given by

$$Z_L = j\omega L \frac{f_1 - \omega^2 f_2}{f_3 - \omega^2 f_4} \quad (9a)$$

$$Z_C = \frac{1}{j\omega} \frac{f_3 - \omega^2 f_4}{f_1 - \omega^2 f_2} \quad (9b)$$

We believe that (8) may be useful for other devices such as microstrip mitered bends, microstrip step junctions, etc.

To display the results in a compact way we define the error in the scattering parameter S_{ij} as the modulus of the difference between the scattering parameter S_{ij}^f computed by the fine model and the scattering parameter S_{ij}^c computed by the coarse model

$$\text{error in } S_{ij} = \left| S_{ij}^f - S_{ij}^c \right| = \sqrt{(\text{Re}[S_{ij}^f] - \text{Re}[S_{ij}^c])^2 + (\text{Im}[S_{ij}^f] - \text{Im}[S_{ij}^c])^2} \quad (10)$$

where $i = 1, 2, \dots, P$ and $j = 1, 2, \dots, P$ (P is the number of ports of the microwave device). We also define the percentage error in S_{ij} by

$$\% \text{ error in } S_{ij} = \left| \frac{S_{ij}^f - S_{ij}^c}{S_{ij}^f} \right| \times 100 \quad (11)$$

We will use percentage error in S_{ij} to display the results whenever $\left| S_{ij}^f \right|$ is not zero.

IV. MULTIVARIABLE RATIONAL FUNCTIONS

Multivariable rational functions (MRFs) [3] are used in most of the modeling examples developed here. A multivariable rational function is the quotient of two polynomials,

$$f(\mathbf{x}, \mathbf{a}, \mathbf{b}) = \frac{a_0 + \sum_{i=1}^n a_i x_i + \sum_{i=1}^n \sum_{j \geq i}^n a_{ij} x_i x_j + \dots}{1 + \sum_{i=1}^n b_i x_i + \sum_{i=1}^n \sum_{j \geq i}^n b_{ij} x_i x_j + \dots} \quad (12)$$

where $\mathbf{x} = [x_1 \ x_2 \ \dots \ x_n]^T$ is the input vector and \mathbf{a} and \mathbf{b} are two vectors containing the unknown a 's and b 's respectively. The polynomials in the numerator and the denominator are of finite order p and q , respectively. The rational function in (12) is fully characterized by the number of input variables n , the numerator order p and the denominator order q , hence we refer to it as $\text{MRF}_{n,p,q}$. The number of unknown parameters in \mathbf{a} and \mathbf{b} can be reduced if some of the input variables are restricted to a certain order less than p or q . For example, a $\text{MRF}_{2,3,2}$ with the order of the input variable x_1 restricted to 1 is given by

$$f(\mathbf{x}, \mathbf{a}, \mathbf{b}) = \frac{a_0 + a_1 x_1 + a_2 x_2 + a_{12} x_1 x_2 + a_{22} x_2^2 + a_{122} x_1 x_2^2 + a_{222} x_2^3}{1 + b_1 x_1 + b_2 x_2 + b_{12} x_1 x_2 + b_{22} x_2^2} \quad (13)$$

which has 11 unknown parameters. On the other hand, the $\text{MRF}_{2,3,2}$ without restricting the order of x_1 has 15 unknown parameters. The unknown parameters in \mathbf{a} and \mathbf{b} can be computed by two methods. First, if the values of the function f in (12) are explicitly available we can evaluate \mathbf{a} and \mathbf{b} by solving an overdetermined system of linear equations. This is done by applying cross-multiplication to both sides of (12) and rearranging the terms to get a system of linear equations in the elements of \mathbf{a} and \mathbf{b} . This system of linear equations can be solved by the method of least-squares or recursive least-squares algorithm [3]. Second, if values of f are not directly available we evaluate \mathbf{a} and \mathbf{b} by solving a suitable optimization problem (in our case the optimization problem in (2)). The second method is adopted in this work since we evaluate the elements of the empirical model (inductors, capacitors, the frequency ω_c , etc.) and the only available information are the scattering parameters supplied by the EM simulators.

V. MODELING EXAMPLES

Microstrip Right Angle Bend

Here, we develop a FIEM and a FDEM for the microstrip right angle bend in Fig. 5(a). The fine model is analyzed by Sonnet's *em* [11] and the coarse model consists of the LC circuit [12] in Fig. 5(b). The vector of input parameters $\mathbf{x}_f = [W \ H \ \varepsilon_r]^T$ and the vector of the circuit elements is $\mathbf{y} = [L/H \ C/H]^T$. Applying dimensional analysis [4,5], we can show that \mathbf{y} is related to \mathbf{x}_f by

$$L/H = \mu_0 f(W/H) \quad (14a)$$

$$C/H = \varepsilon_0 f(W/H, \varepsilon_r) \quad (14b)$$

Therefore, \mathbf{y} is a function of $\mathbf{x}_r = [W/H \ \varepsilon_r]^T$. We first develop a FIEM in the frequency range [1, 11] GHz. The region of interest is $0.2 < W/H < 6$ and $2 < \varepsilon_r < 11$. The substrate height H is chosen in the range [5, 30] mil. We use a three-layer perceptron ANN (with hyperbolic-tangent as nonlinear activation function) to approximate \mathbf{y} . Two hidden neurons were used for L/H and three hidden neurons for C/H . The training points are chosen according to the Central Composite Design (CCD) [9] in addition to 4 more points as shown in Fig. 6 (total 13 training points) where \hat{x}_1 and \hat{x}_2 are the scaled input variables

corresponding to W/H and ϵ_r , respectively. The vector \mathbf{y} is also approximated by MRFs. The inductance per unit length L/H is approximated by a rational function $\text{MRF}_{2,2,2}$ and the capacitance per unit length C/H is approximated by a rational function of order $\text{MRF}_{2,3,0}$ with the order of W/H restricted to one (this gives better generalization performance than if we did not restrict the order of W/H). The parameters of the ANNs and the MRFs are obtained by the Huber optimizer in OSA90/hope [13]. Figs. 7(a) and (b) show the error in the scattering parameter S_{11} at 16 test points in the region of interest for the FIEM developed by ANN and MRF, respectively. Fig. 7(c) shows the corresponding error due to the Jansen model [14] at the same test points. We see that the three models are comparable.

The results obtained by the FIEM (developed by either ANNs or MRFs) and by the Jansen empirical model [14] over the range [1, 31] GHz are shown in Figs. 8 (a), (b) and (c), respectively. It is clear that neither the FIEM nor the empirical model in [14] are accurate at high frequencies. Therefore, we develop a FDEM (see Fig. 4), where ω_c is a function of ω and the other parameters. Applying dimensional analysis (see Appendix A) and using the odd property of ω_c we get

$$\omega_c = \omega \gamma(\mathbf{x}_r, (\omega H/c)^2) \quad (15)$$

where c is the speed of light and γ is an unknown function to be approximated. We use MRFs to approximate \mathbf{y} as well as ω_c . A $\text{MRF}_{3,2,2}$ with the order of $(\omega H/c)^2$ restricted to one is used to approximate ω_c . The number of training points used to develop the FDEM is the same as that used to develop the FIEM. Figs. 9 (a) and (b) show the errors in the scattering parameters S_{11} and S_{21} at 16 test points in the region of interest for the FDEM. Fig. 10 compares the results obtained by the FDEM and those from Sonnet's *em* [11]. The empirical expressions for \mathbf{y} and ω_c are given in Table I (Appendix B).

We transform the FDEM into an equivalent FIEM as follows. The frequency ω_c is given by (8) and, hence the impedances associated with L and C are given by (9a) and (9b), respectively. These impedances are realized by the first Foster realization [8]. The equivalent FIEM is shown in Fig. 11(b), where all elements are frequency independent and functions only of the device parameters.

Microstrip Via

Here, we consider modeling the microstrip via of Fig. 12(a). The coarse model is an inductor L to ground (Fig. 12(b)). The fine model is analyzed by Sonnet's *em* [11]. The reference plane is at the junction of the microstrip line and the square pad. The vector $\mathbf{x}_f = [W \ H \ W_0 \ D]^T$, where H is the substrate height (GaAs, $\epsilon_r=12.9$). Here, $\mathbf{y} = [L/H]$, which is given by

$$L/H = \mu_0 \ f(W/H, W_0/W, D/W) \quad (16)$$

hence, $\mathbf{x}_r = [W/H \ W_0/W \ D/W]^T$. A FIEM was developed in the range [2, 10] GHz. The region of interest is $1 < W/H < 2.2$, $0.2 < W_0/W < 1$ and $0.2 < D/W < 0.8$. We use a $\text{MRF}_{3,2,2}$ to approximate L/H . The training points are chosen according to the Central Composite Design (CCD) [9] in addition to 8 more points (total 23 training points). The parameters of the MRF are obtained by the Huber optimizer in OSA90/hope [13]. The percentage errors in the inductance L and in S_{11} at 30 test points are shown in Fig. 13. Fig. 14 compares the FIEM with Sonnet's *em* [11]

The results of the FIEM in the range [2, 22] GHz are shown in Fig. 15. We notice large errors at high frequencies. This is because the simple inductor to ground does not take into account the effect of the pad surrounding the via hole and the step junction [15] (see Fig. 12). To overcome this deficiency we develop a FDEM in the range [2, 22] GHz. The coarse model frequency (applying dimensional analysis and using the odd property of the frequency mapping) takes the same form as in (15). We use MRFs to approximate \mathbf{y} as well as ω_c . The number of training points used is 23. The percentage errors in L and in S_{11} at 30 test points are shown in Figs. 16 (a) and (b), respectively. The empirical expressions for L and ω_c are given in Table II (Appendix B). The transformation of the FDEM into an equivalent FIEM follows the microstrip right angle bend example. The frequency ω_c is given by (8). The equivalent impedance of L is of the form of (9a). The resulting FIEM is shown in Fig. 17: it has the same topology as the broadband model suggested by [16].

Microstrip Double-Step

Here, we consider broadband modeling of the microstrip double-step element in Fig. 18(a). It can be used to model microstrip tapered lines or nonuniform (in width) microstrip lines. The coarse model consists of two shunt capacitances and one series inductance (see Fig. 18(b)). The fine model is analyzed by Sonnet's *em* [11]. The vector of fine model parameters $\mathbf{x}_f = [W_1 \ W_2 \ W_3]^T$. The substrate height $H=25$ mil, the relative dielectric constant $\epsilon_r = 9.7$ and the length l (see Fig. 18(a)) is 5 mil. The circuit elements vector $\mathbf{y} = [L_1/H \ C_1/H \ C_2/H]^T$. The elements of \mathbf{y} are given by

$$L_1/H = \mu_0 f_1\left(\frac{W_2}{H}, \frac{W_2}{W_1}, \frac{W_3}{W_2}\right) \quad (17a)$$

$$C_1/H = \epsilon_0 f_2\left(\frac{W_2}{H}, \frac{W_2}{W_1}, \frac{W_3}{W_2}\right) \quad (17b)$$

$$C_2/H = \epsilon_0 f_3\left(\frac{W_2}{H}, \frac{W_2}{W_1}, \frac{W_3}{W_2}\right) \quad (17c)$$

hence, $\mathbf{x}_r = [W_2/H \ W_2/W_1 \ W_3/W_2]^T$. The coarse model frequency (applying dimensional analysis and using the odd property of the frequency mapping) takes the same form as in (15). A FDEM of the double-step element is developed in the range [1, 41] GHz. The region of interest is $0.1 < W_2/H < 1$, $0.5 < W_2/W_1 < 0.9$ and $0.5 < W_3/W_2 < 0.9$. We use a $\text{MRF}_{3,2,2}$ to approximate each element of the vector \mathbf{y} and a $\text{MRF}_{4,2,2}$ to approximate ω_c with the order of $(\omega H/c)^2$ restricted to 1. The number of training points is 23. The parameters of the MRFs are obtained by the Huber optimizer in OSA90/hope [13]. The empirical expressions for \mathbf{y} and ω_c are given in Table III (Appendix B). The errors in S_{11} and S_{21} of the FDEM with respect to Sonnet's *em* [11] at 27 testing points in the region of interest are shown in Figs. 19 (a) and (b), respectively. To evaluate the FDEM of the double-step we consider an alternative model for the double-step element. This model is composed of a microstrip transmission line and 2 step junctions as shown in Fig. 20. The empirical models for the microstrip line and the 2 step junctions are taken from OSA90/hope. Figs. 21(a) and (b) show the errors in S_{11} and S_{21} of this model with respect to Sonnet's *em* [11] at 27 testing points in the region of interest. It is clear from Figs. 19 and 21 that the FDEM outperforms the double-step model in Fig. 20.

The FDEM of the double-step element is used to model the linear tapered microstrip line in Fig. 22. The parameters of the tapered line are $L=150$ mil, $W_{in}=18$ mil, $W_{out}=2$ mil, $H=25$ mil and $\epsilon_r = 9.7$. The input microstrip line has a characteristic impedance of 50 ohm and the output line has a characteristic impedance of 100 ohm. The linear tapered microstrip line can be analyzed by cascading 30 double-step elements (each of length $l=5$ mil). The ABCD matrix of the tapered line is related to the ABCD matrices of the double-step elements by

$$\begin{bmatrix} A & B \\ C & D \end{bmatrix} = \prod_{i=1}^{30} \begin{bmatrix} A_i & B_i \\ C_i & D_i \end{bmatrix} \quad (18)$$

We analyzed the tapered line by three methods: by Sonnet's *em* [11] (the fine model), by cascading 30 double-step elements, where the FDEM is used to model each element and by cascading 30 elements where the alternative model of the double-step element (Fig. 20) is used. Fig. 23 compares the results obtained by the three methods.

CPW Step Junction

Here, we develop a FIEM for the CPW step junction in Fig. 24(a). The fine model is analyzed by Sonnet's *em* [11] and the coarse model consists of the LC circuit [12] in Fig. 5(b). The vector of input parameters $\mathbf{x}_f = [W_1 \ W_2 \ G]^T$ and the vector of the circuit elements is $\mathbf{y} = [L_1/H \ L_2/H \ C/H]^T$, where

$$L_1 / H = \mu_0 \ f_1(W_1/H, W_2/W_1, G/W_1) \quad (19a)$$

$$L_2 / H = \mu_0 \ f_2(W_1/H, W_2/W_1, G/W_1) \quad (19b)$$

$$C / H = \epsilon_0 \ f_3(W_1/H, W_2/W_1, G/W_1) \quad (19c)$$

Therefore, \mathbf{y} is a function of $\mathbf{x}_r = [W_1/H \ W_2/W_1 \ G/W_1]^T$. The region of interest is $40 \mu\text{m} < W_1 < 120 \mu\text{m}$, $0.2 < W_2/W_1 < 0.8$ and $0.2 < G/W_1 < 1$ and the frequency range is [5, 50] GHz. The substrate height H is 635 μm and the relative dielectric constant is $\epsilon_r = 12.9$ (GaAs). The number of training points is 23. Each element of the vector \mathbf{y} is approximated by a rational function $\text{MRF}_{3,2,2}$. The parameters of the MRFs are obtained by the Huber optimizer in OSA90/hope [13]. The expressions for the elements of \mathbf{y} are given in Table IV (Appendix B). Figs. 25 (a) and (b) compares between the results obtained by *em* [11] and those

by the CPW step junction FIEM at 27 test points in the region of interest. We notice that the CPW step junction FIEM gives good results in broad frequency range 5 GHz to 50 GHz. Therefore, we do not need to develop a FDEM for the CPW step junction. This means that the elements of the CPW step junction empirical model are frequency independent. Fig. 26 compares between the capacitance C extracted from the Z-parameters obtained by *em* [11] (actually, *em* gives the S-parameters which can be transformed to Z-parameters) using the formula

$$C(pf) = -10^3 / (\text{Im}[Z_{21}] \omega(\text{GHz})) \quad (20)$$

where $\text{Im}[Z_{21}]$ is the imaginary part of the Z_{21} and that predicted by the FIEM of the CPW step junction at 6 test points in the region of interest.

VI. CONCLUSIONS

We present a unified computer-aided modeling methodology for developing broadband models of microwave passive components. Our approach integrates in a coherent way full-wave EM simulations, artificial neural networks, multivariable rational functions, dimensional analysis and frequency mapping. Two types of models are considered: FIEMs and FDEMs. FDEMs can be transformed to equivalent FIEMs if we use a MRF to approximate the frequency mapping. This is important since the FIEMs are readily implementable in conventional circuit simulators. We applied our modeling methodology to develop broadband empirical models for several microwave components, including a microstrip right angle bend, a microstrip via, a microstrip double-step (to be used as a basic element of constructing a coarse model for nonuniform or tapered microstrip transmission lines) and a CPW step junction.

Appendix A

We apply dimensional analysis to determine the dependency of the coarse model frequency ω_c of the microstrip right angle bend FDEM on the fine model frequency ω and the other parameters (see Fig. 5). The method of dimensional analysis is based on Buckingham's theorem [4]. This theorem states that "If an equation is dimensionally homogeneous it can be reduced to a relationship among a complete set of

dimensionless products of the system variables". The dimensionless products are called Pi (π) terms [4,5].

For our case we assume that ω_c depends on ω , the device parameters W, H, ε , the free space permittivity ε_0 and the speed of light c (we can replace c with the free space permeability μ_0). A dimensional product π takes the form

$$\pi = H^{x_1} W^{x_2} c^{x_3} \varepsilon^{x_4} (\varepsilon_0)^{x_5} \omega^{x_6} (\omega_c)^{x_7} \quad (\text{A.1})$$

where the x 's are evaluated by solving the system of homogeneous equations

$$\mathbf{C} \mathbf{x} = 0 \quad (\text{A.2})$$

The elements of the coefficient matrix \mathbf{C} in (A.2) can be obtained by constructing the table [4]

	x_1	x_2	x_3	x_4	x_5	x_6	x_7
	H	W	C	ε	ε_0	ω	ω_c
Kg	0	0	0	-1	-1	0	0
M	1	1	1	-3	-3	0	0
S	0	0	-1	4	4	-1	-1
A	0	0	0	2	2	0	0

where Kg, M, S and A are the units of the SI system. Therefore, \mathbf{C} is given by

$$\mathbf{C} = \begin{bmatrix} 0 & 0 & 0 & -1 & -1 & 0 & 0 \\ 1 & 1 & 1 & -3 & -3 & 0 & 0 \\ 0 & 0 & -1 & 4 & 4 & -1 & -1 \\ 0 & 0 & 0 & 2 & 2 & 0 & 0 \end{bmatrix} \quad (\text{A.3})$$

The number of independent solutions of (A.2) (the same as the number of independent π -terms) equals the number of elements of \mathbf{x} in (A.2) minus the rank of the matrix \mathbf{C} . In our case the number of elements of \mathbf{x} is 7 and the rank of the matrix \mathbf{C} is 3, hence we have 4 independent solutions of (A.2) or 4 π -terms. These independent solutions are given in the table

x_1	x_2	x_3	x_4	x_5	x_6	x_7
1	0	-1	0	0	1	0
0	1	-1	0	0	1	0
0	0	0	-1	1	0	0
0	0	0	0	0	-1	1

Therefore, the π -terms are given by

$$\pi_1 = \omega H / c, \quad \pi_2 = \omega W / c, \quad \pi_3 = \varepsilon / \varepsilon_0 = \varepsilon_r, \quad \pi_4 = \omega_c / \omega \quad (\text{A.4})$$

from π_1 and π_2 we can get $\pi_2' = \pi_2 / \pi_1 = W / H$. Applying Buckingham's theorem [4,5] the relation between the independent π -terms can take the form

$$\pi_4 = \varphi(\pi_1, \pi_2', \pi_3) \quad (\text{A.5})$$

Therefore,

$$\omega_c = \omega \varphi(W/H, \varepsilon_r, \omega H/c) \quad (\text{A.5})$$

But since ω_c is an odd function of ω (see Section III) we get

$$\omega_c = \omega f(W/H, \varepsilon_r, (\omega H/c)^2) \quad (\text{A.6})$$

TABLE I
EXPRESSIONS OF THE ELEMENTS OF THE FDEM
OF THE MICROSTRIP RIGHT ANGLE BEND

Element	Expression
$L/H(\text{nH}/\text{mil})$	$0.03192 \frac{-0.09 - 0.018x_1 + 0.3x_1^2}{1 + 2.853x_1^2}$
$C/H(\text{pF}/\text{mil})$	$0.000225(-0.46 + 0.162x_1 - 0.014x_2 + 0.275x_1^2 + 2.855x_1x_2 + 0.262x_1^2x_2)$
ω_c/ω	$\frac{f_1(x_1, x_2, x_3)}{f_2(x_1, x_2, x_3)}$
	$f_1(x_1, x_2, x_3) = 0.759 - 0.0192x_1 - 0.0179x_2 + 0.0187x_3 + 0.0738x_1^2 + 0.0026x_1x_2$ $- 0.1405x_1x_3 + 0.0079x_2x_3 + 0.0018x_1^3 - 0.0071x_1^2x_2 + 0.1188x_1^2x_3$ $+ 0.0017x_1x_2^2 + 0.0419x_1x_2x_3 - 0.0022x_2^2x_3$
	$f_2(x_1, x_2, x_3) = 1 + 0.0282x_1 - 0.0086x_2 - 0.0175x_3 + 0.0051x_1^2 - 0.0063x_1x_2$ $+ 0.1674x_1x_3 + 0.0037x_2^2 - 0.0067x_2x_3 + 0.0055x_1^3 - 0.0028x_1^2x_2$ $+ 0.0011x_1^2x_3 + 0.0056x_1x_2x_3 - 0.0012x_2^2x_3$
	where $x_1 = W/H$, $x_2 = \epsilon_r$, $x_3 = 1.816e - 7 (\omega(\text{GHz})H(\text{mil}))^2$

TABLE II
EXPRESSIONS OF THE ELEMENTS OF
THE FDEM OF THE MICROSTRIP VIA

Element	Expression
$L/H(\text{nH}/\text{mil})$	$0.03192 \frac{f_1(x_1, x_2, x_3)}{f_2(x_1, x_2, x_3)}$
	$f_1(x_1, x_2, x_3) = 0.0123 + 2.173x_1 + 14.166x_2 + 1.779x_3 + 1.875x_1^2 - 5.036x_1x_2$ $- 0.983x_1x_3 - 8.622x_2^2 - 2.111x_2x_3$
	$f_2(x_1, x_2, x_3) = 1 - 3.835x_1 + 30.784x_2 + 3.26x_3 + 7.161x_1^2 + 15.471x_1x_2$ $- 1.088x_1x_3 - 21.862x_2^2 - 7.381x_2x_3$
ω_c/ω	$\frac{f_3(x_1, x_2, x_3, x_4)}{f_4(x_1, x_2, x_3, x_4)}$
	$f_3(x_1, x_2, x_3, x_4) = 0.9156 - 0.0427x_1 - 0.065x_2 - 0.3837x_3 - 0.2494x_4$ $- 0.0948x_1^2 - 0.0979x_1x_2 + 0.0808x_1x_3 + 0.0095x_1x_4 + 0.161x_2^2$ $+ 0.1121x_2x_3 + 0.5776x_2x_4 + 0.0962x_3^2 + 0.0108x_3x_4$
	$f_4(x_1, x_2, x_3, x_4) = 1 - 0.2841x_1 + 0.0418x_2 - 0.2042x_3 - 0.4723x_4$ $- 0.024x_1^2 - 0.1315x_1x_2 + 0.0649x_1x_3 + 0.0342x_1x_4 + 0.1864x_2^2$ $+ 0.101x_2x_3 + 0.885x_2x_4 - 0.0029x_3^2 + 0.0725x_3x_4$
	where $x_1 = W/H$, $x_2 = D/W$, $x_3 = W_0/W$, $x_4 = 1.816e - 07 (\omega(\text{GHz})H(\text{mil}))^2$

TABLE III
EXPRESSIONS OF THE ELEMENTS OF
THE FDEM OF THE MICROSTRIP DOUBLE-STEP

Element	Expression
$C_1/H(\text{pF}/\text{mil})$	$0.0002246 \frac{f_1(x_1, x_2, x_3)}{f_2(x_1, x_2, x_3)}$ $f_1(x_1, x_2, x_3) = 0.6433 + 0.6697x_1 - 0.4604x_2 + 0.0088x_3 - 0.7741x_1^2$ $+ 0.099x_1x_2 + 0.3921x_1x_3 - 0.2749x_2^2 + 0.1779x_2x_3 - 0.0642x_3^2$ $f_2(x_1, x_2, x_3) = 1 + 0.5641x_1 - 0.3232x_2 - 0.0211x_3 - 0.6742x_1^2 + 0.0499x_1x_2$ $+ 0.4428x_1x_3 - 0.5845x_2^2 + 0.0087x_2x_3 - 0.2907x_3^2$
$C_2/H(\text{pF}/\text{mil})$	$0.0002246 \frac{f_3(x_1, x_2, x_3)}{f_4(x_1, x_2, x_3)}$ $f_1(x_1, x_2, x_3) = 0.7485 + 3.0972x_1 + 0.1092x_2 - 0.3263x_3 - 0.0003x_1^2$ $+ 0.2666x_1x_2 + 1.0371x_1x_3 + 0.2595x_2^2 + 0.3725x_2x_3 - 0.5347x_3^2$ $f_2(x_1, x_2, x_3) = 1 - 0.6556x_1 - 0.1716x_2 - 1.1229x_3 - 0.025x_1^2 + 0.4179x_1x_2$ $+ 0.4398x_1x_3 + 0.0063x_2^2 + 1.897x_2x_3 + 0.0122x_3^2$
$L/H(\text{nH}/\text{mil})$	$0.03192 \frac{f_5(x_1, x_2, x_3)}{f_6(x_1, x_2, x_3)}$ $f_5(x_1, x_2, x_3) = 0.2934 + 0.2522x_1 - 0.2209x_2 - 0.1631x_3 - 0.0737x_1^2$ $- 0.0891x_1x_2 - 0.1021x_1x_3 + 0.1401x_2^2 - 0.0169x_2x_3 + 0.117x_3^2$ $f_6(x_1, x_2, x_3) = 1 + 2.5332x_1 + 0.066x_2 + 0.6713x_3 - 1.111x_1^2 + 0.7775x_1x_2$ $- 0.1045x_1x_3 - 0.1237x_2^2 - 0.8642x_2x_3 - 0.3023x_3^2$
ω_c/ω	$\frac{f_5(x_1, x_2, x_3, x_4)}{f_6(x_1, x_2, x_3, x_4)}$ $f_3(x_1, x_2, x_3, x_4) = 0.8955 - 0.2519x_1 + 0.0699x_2 + 0.2416x_3 - 0.076x_4$ $- 0.1473x_1^2 + 0.2027x_1x_2 - 0.3735x_1x_3 + 0.0583x_1x_4 - 0.0602$ $- 0.0456x_2x_3 + 0.0499x_2x_4 + 0.1394x_3^2 - 0.0257x_3x_4$ $f_6(x_1, x_2, x_3, x_4) = 1 + 0.0524x_1 - 0.1599x_2 + 0.0579x_3 - 0.0748x_4$ $- 0.1895x_1^2 - 0.0577x_1x_2 - 0.5079x_1x_3 + 0.064x_1x_4 + 0.1261x_2^2$ $+ 0.1076x_2x_3 + 0.0389x_2x_4 + 0.2899x_3^2 - 0.0373x_3x_4$
<p>where</p> $x_1 = W_2 / H, \quad x_2 = W_2 / W_1, \quad x_3 = W_3 / W_2, x_4 = 1.816e - 07 (\omega(\text{GHz})H(\text{mil}))^2$	

TABLE IV
EXPRESSIONS OF THE ELEMENTS OF
THE FIEM OF THE CPW STEP JUNCTION

Element	Expression
L_1/H (nH/ μm)	$0.00126 \frac{f_1(x_1, x_2, x_3)}{f_2(x_1, x_2, x_3)}$ $f_1(x_1, x_2, x_3) = 0.0236 - 0.0222x_1 - 0.0013x_2 - 0.0114x_3 + 0.1257x_1^2 + 0.0045x_1x_2 - 0.0131x_1x_3 - 0.0099x_2^2 + 0.0147x_2x_3 - 0.0092x_3^2$ $f_2(x_1, x_2, x_3) = 1 + 0.0909x_1 + 0.4219x_2 - 0.9638x_3 + 0.1791x_1^2 + 0.0011x_1x_2 + 0.5169x_1x_3 - 0.0372x_2^2 - 0.1109x_2x_3 - 0.0045x_3^2$
L_2/H (nH/ μm)	$0.00126 \frac{f_3(x_1, x_2, x_3)}{f_4(x_1, x_2, x_3)}$ $f_3(x_1, x_2, x_3) = 0.0246 + 0.0782x_1 - 0.0496x_2 + 0.0175x_3 - 0.3558x_1^2 - 0.0523x_1x_2 + 0.1423x_1x_3 + 0.0415x_2^2 + 0.0192x_2x_3 - 0.0122x_3^2$ $f_4(x_1, x_2, x_3) = 1 - 1.3664x_1 + 0.2942x_2 + 0.2462x_3 - 0.511x_1^2 - 0.0126x_1x_2 - 0.1033x_1x_3 + 0.1729x_2^2 + 1.0585x_2x_3 - 0.4105x_3^2$
C/H (pF/ μm)	$8.842e - 06 \frac{f_5(x_1, x_2, x_3)}{f_6(x_1, x_2, x_3)}$ $f_5(x_1, x_2, x_3) = 1.7 - 1.8175x_1 + 0.0193x_2 - 0.0039x_3 + 0.1988x_1^2 - 2.5228x_1x_2 + 0.5604x_1x_3 + 0.0358x_2^2 + 2.3426x_2x_3 + 0.873x_3^2$ $f_6(x_1, x_2, x_3) = 1 - 2.9222x_1 - 0.5578x_2 + 0.7102x_3 - 1.2069x_1^2 + 1.6552x_1x_2 + 1.0808x_1x_3 + 0.0459x_2^2 + 0.9144x_2x_3 + 0.8377x_3^2$ <p style="margin-left: 20px;">where $x_1 = W_1 / H$, $x_2 = W_2 / W_1$, $x_3 = G / W_1$</p>

ACKNOWLEDGEMENT

The authors thank Dr. J.C. Rautio, President, Sonnet Software, Inc., Liverpool, NY, for making *em*TM available.

REFERENCES

- [1] A.H. Zaabab, Q.J. Zhang and M.S. Nakhala, "A neural network modeling approach to circuit optimization and statistical design," *IEEE Trans. Microwave Theory Tech.*, vol. 43, 1995, pp. 1349-1358.
- [2] P. Watson and K.C. Gupta, "EM-ANN models for microstrip vias and interconnects in multilayer circuits," *IEEE Trans. Microwave Theory Tech.*, vol. 44, 1996, pp. 2495-2503.

- [3] H. Leung and S. Haykin, "Rational function neural network," *Neural Computation*, vol. 5, 1993, pp. 928-938.
- [4] W.H. Middelndorf, *Design of Devices and Systems*. New York: Marcel Dekker, Inc., 1986, Chapter 7.
- [5] P. Watson, M.Y. Mah and L.L. Liou, "Input variable space reduction using dimensional analysis for artificial neural network modeling," *IEEE MTT-S Int. Microwave Symp. Dig.* (Anaheim, CA), 1999, pp. 269-272.
- [6] J.W. Bandler, R.M. Biernacki, S.H. Chen, R.H. Hemmers and K. Madsen, "Electromagnetic optimization exploiting aggressive space mapping," *IEEE Trans. Microwave Theory Tech.*, vol. 43, 1995, pp. 2874-2882.
- [7] J.W. Bandler, M.A. Ismail, J.E. Rayas-Sánchez and Q.J. Zhang, "Neuromodeling of microwave circuits exploiting space mapping technology," *IEEE Trans. Microwave Theory Tech.*, vol. 47, 1999, pp. 928-938.
- [8] G.C. Temes and J.W. Lapatra, *Introduction to Circuit Synthesis and Design*. New York: McGraw-Hill, Inc., 1977.
- [9] D.C. Montgomery, *Design and Analysis of Experiments*. New York: Wiley, 1991.
- [10] R. Collin, *Foundations for Microwave Engineering*. New York: McGraw-Hill, Inc., 1966.
- [11] *em*TM Version 4.0b, Sonnet Software, Inc., 1020 Seventh North Street, Suite 210, Liverpool, NY 13088, 1997.
- [12] K.C. Gupta, R. Garg, I.J. Bahl, *Microstrip Lines and Slotlines*. Dedham, MA: Artech House, 1979.
- [13] OSA90/hopeTM Version 4.0, formerly Optimization Systems Associates Inc., P.O. Box 8083, Dundas, Ontario, Canada L9H 5E7, now Agilent Technologies, 1400 Fountaingrove, Parkway, Santa Rosa, CA 95403-1799.
- [14] M. Kirschning, R. Jansen and N. Koster, "Measurement and computer-aided modeling of microstrip discontinuities by an improved resonator method," *IEEE MTT-S Int. Microwave Symp. Dig.* (Boston, MA), 1983, pp. 495-497.
- [15] D.G. Swanson, Jr., "Grounding microstrip lines with via holes," *IEEE Trans. Microwave Theory Tech.*, vol. 40, 1992, pp. 1719-1721.
- [16] D.G. Swanson, Jr., "EM field simulators made practical," Field-Solver Course, M/A-COM Division of AMP, Lowell, MA, 1998.

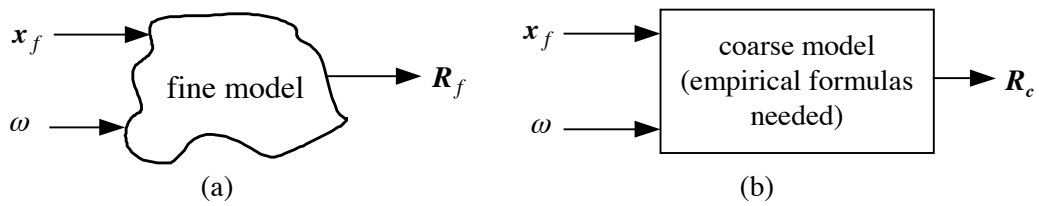


Fig. 1. The fine model (a) and the coarse model (b).

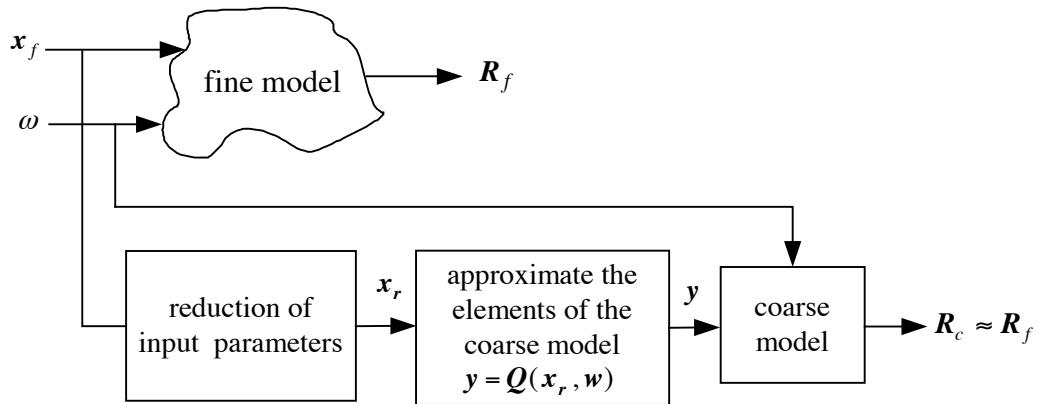


Fig. 2. The development of the frequency-independent empirical model (FIEM).

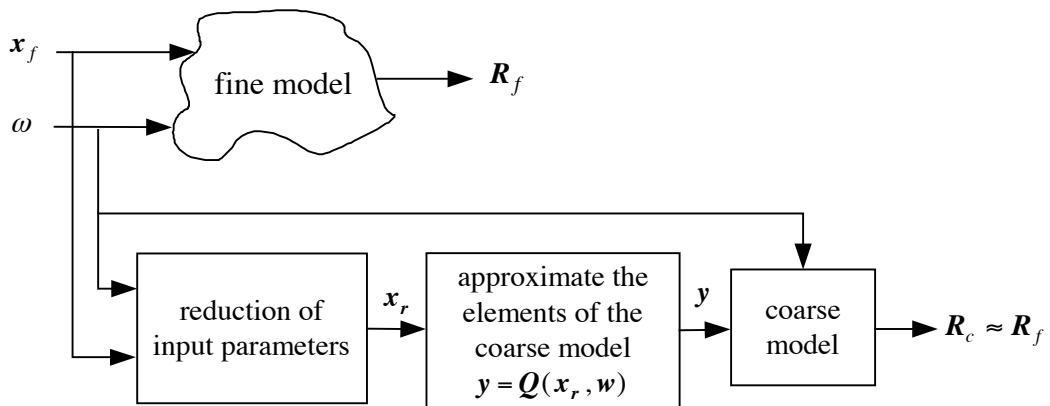


Fig. 3. The development of the FDEM with elements explicitly function of frequency.

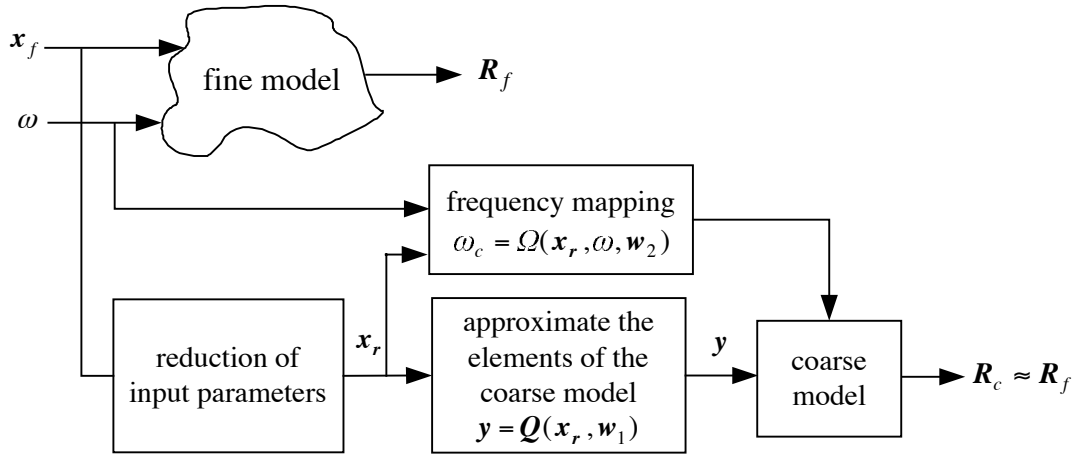


Fig. 4. The development of the FDEM with elements implicitly function of frequency through frequency mapping.

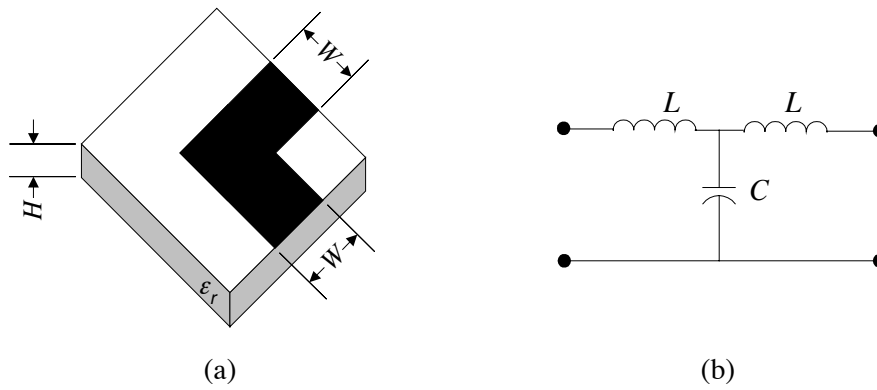


Fig. 5. The microstrip right angle bend: (a) the fine model, (b) the coarse model.

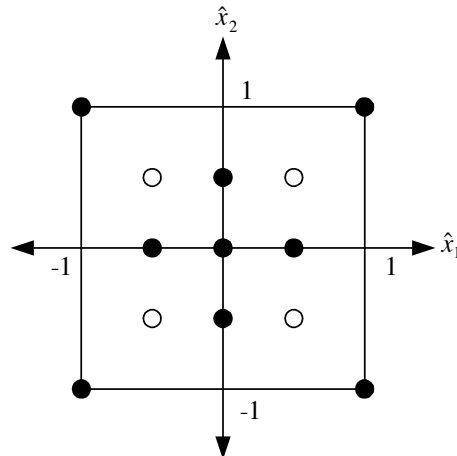


Fig. 6. The training points for the microstrip right angle bend.

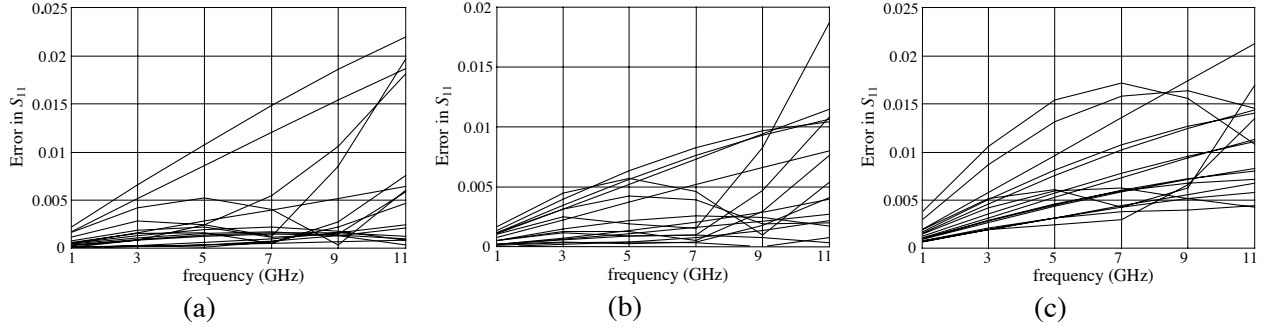


Fig. 7. The error in S_{11} of the microstrip right angle bend with respect to em^{TM} at the test points: (a) the FIEM developed by ANNs, (b) the FIEM developed by MRFs, (c) by the empirical model in [14].

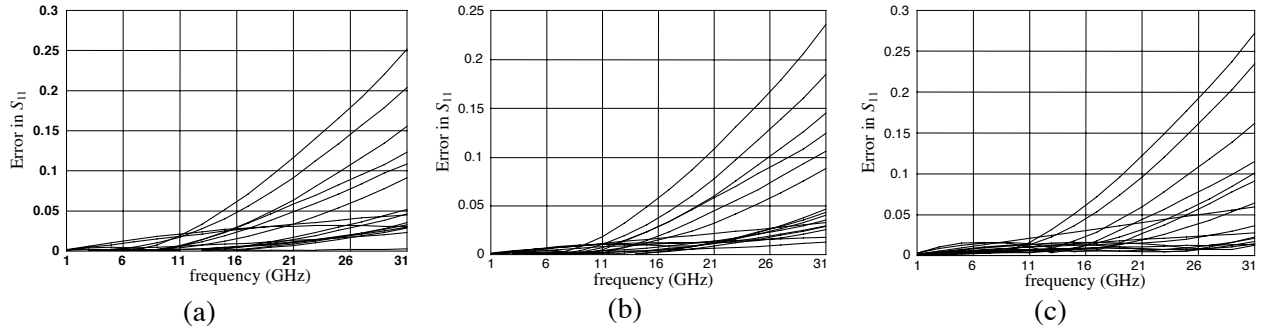


Fig. 8. The error in S_{11} of the microstrip right angle bend with respect to em^{TM} over a broad frequency range: (a) the FIEM developed by ANNs, (b) the FIEM developed by MRFs, (c) the empirical model in [14].

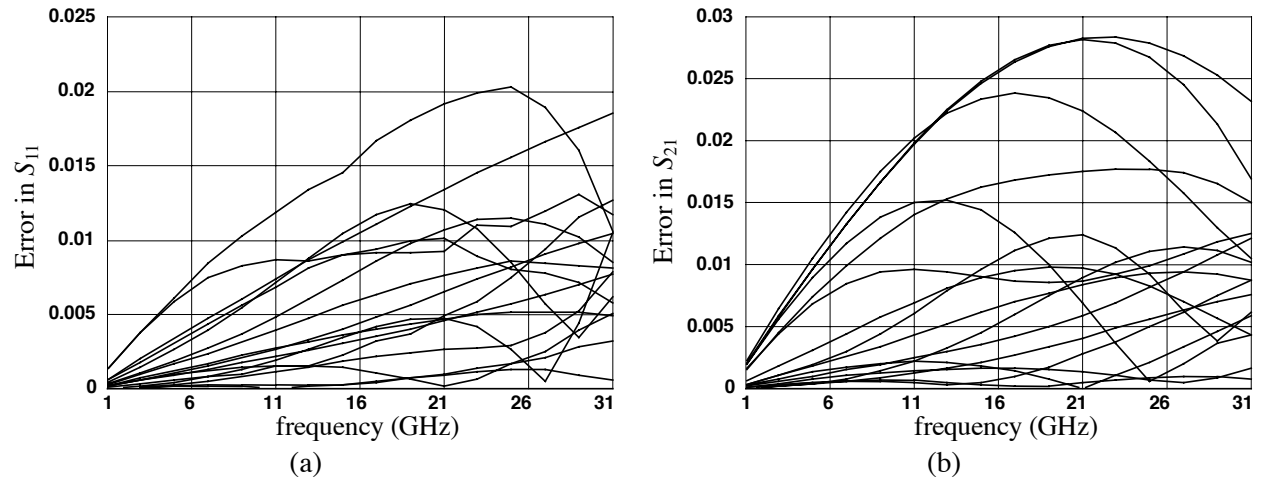


Fig. 9. Error of the FDEM of the microstrip right angle bend (developed by MRFs) with respect to em^{TM} at the test points: (a) in S_{11} , (b) in S_{21} .

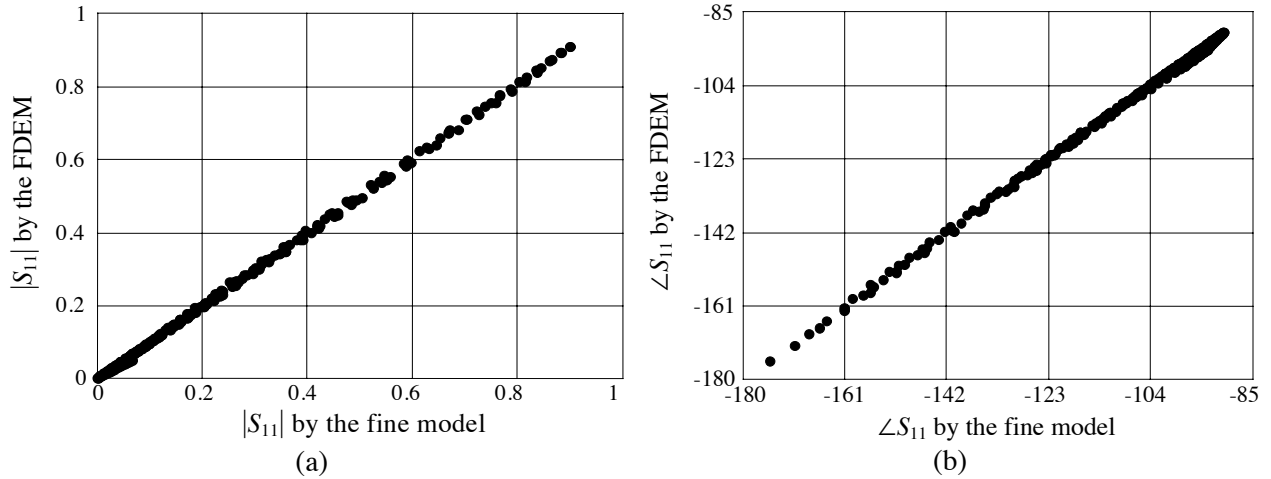


Fig. 10. Comparison between the responses obtained by the FDEM of the microstrip right angle bend and those obtained by em^{TM} at the test points: (a) magnitude of S_{11} , (b) phase of S_{11} in degrees.

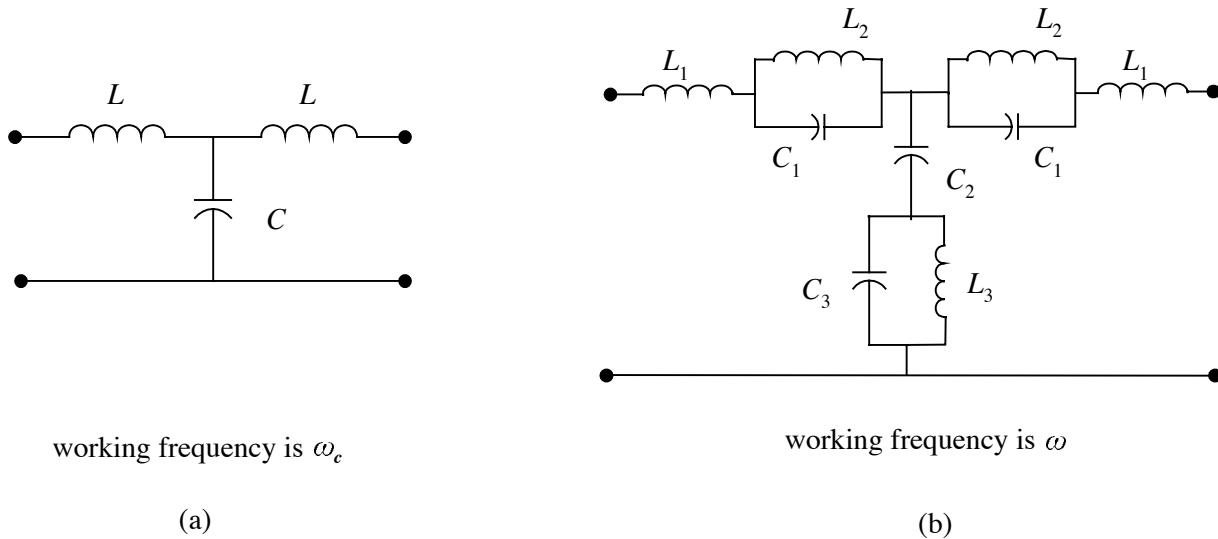


Fig. 11. The FDEM of the microstrip right angle bend (a) and the equivalent FIEM (b).

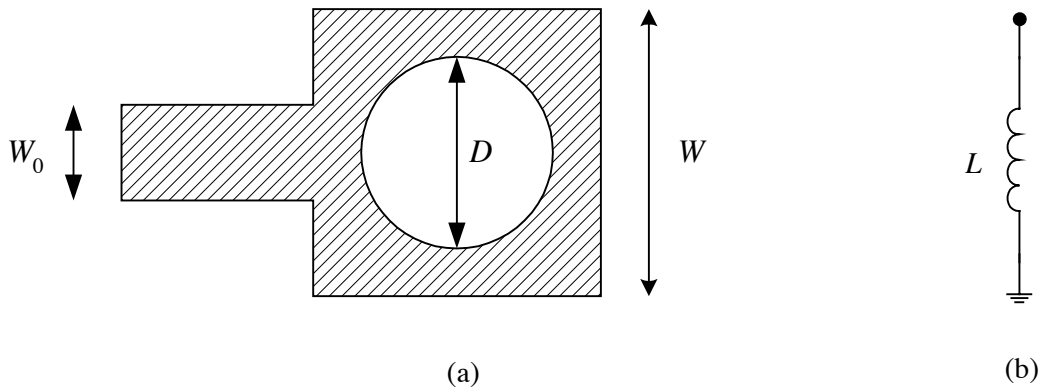


Fig. 12. The microstrip via: (a) the physical structure, (b) the coarse model (equivalent circuit).

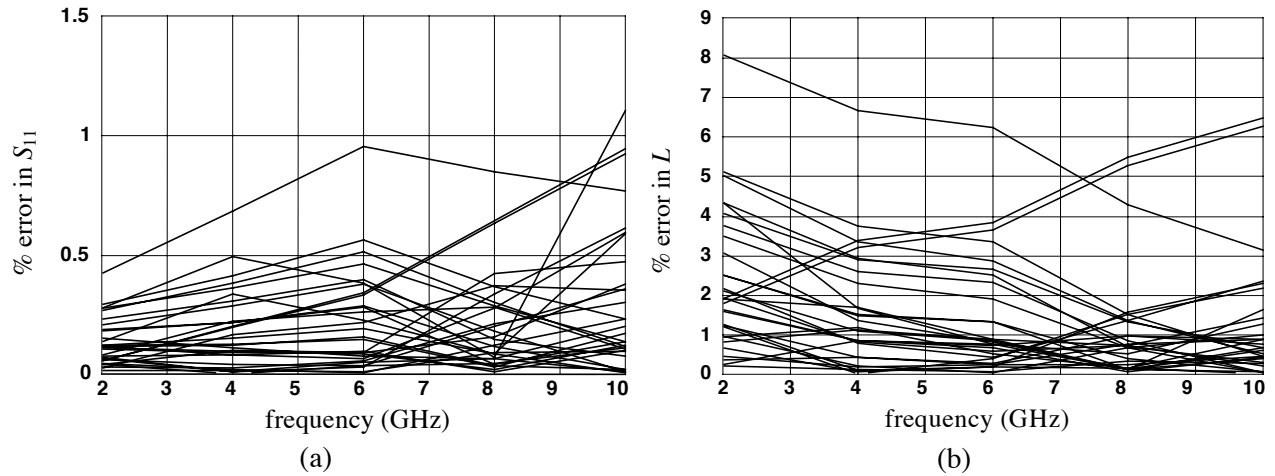


Fig. 13. Percentage error of the FIEM of the microstrip via with respect to em^{TM} at the test points: (a) in S_{11} , (b) in L .

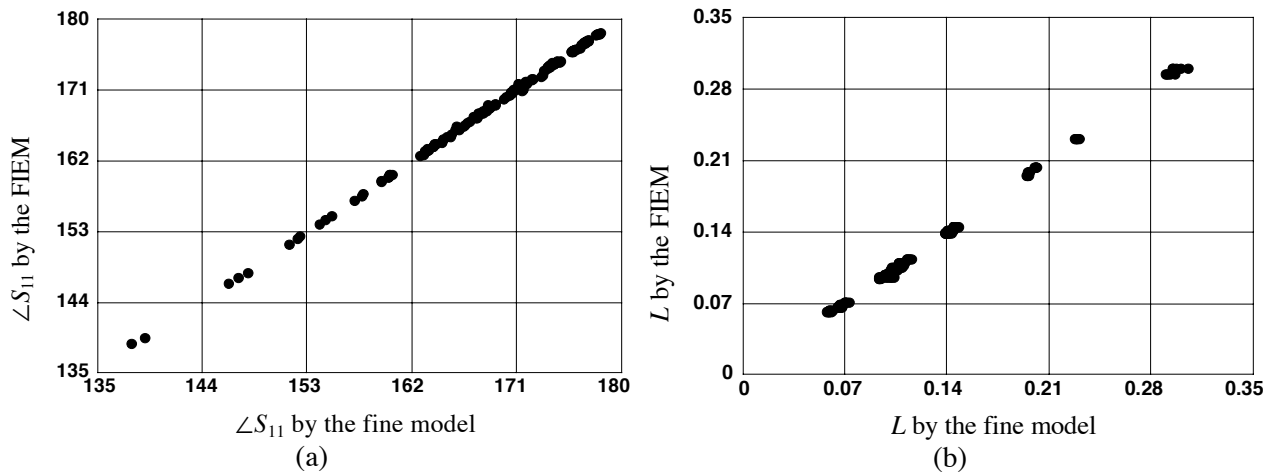


Fig. 14. Comparison between the responses obtained by the FIEM of the microstrip via and those obtained by em^{TM} at the test points in the frequency range [2, 10] GHz: (a) phase of S_{11} , (b) the inductance L .

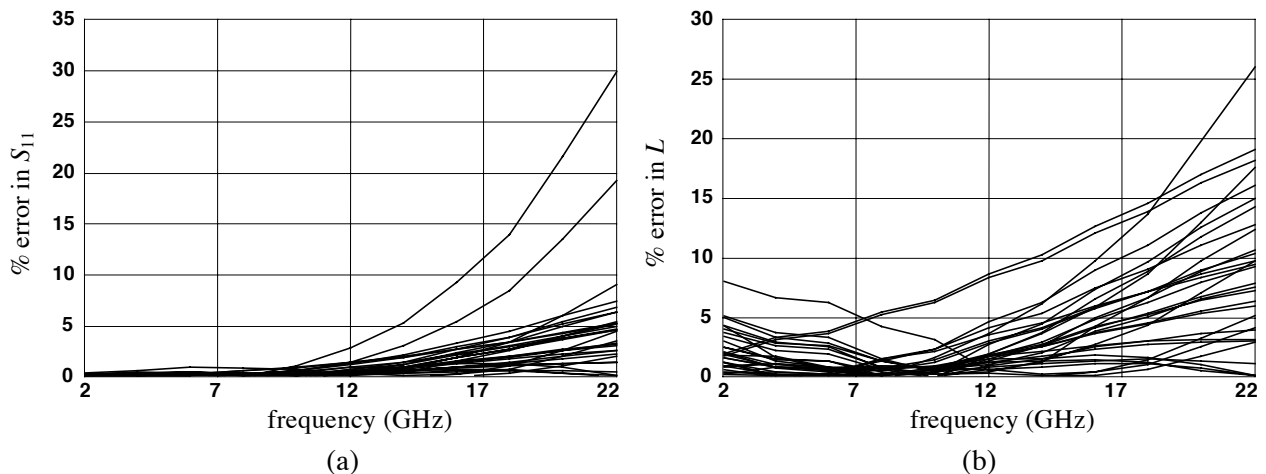


Fig. 15. Comparison of the FIEM of the microstrip via with respect to em^{TM} over a broad frequency range at the test points: (a) % error in S_{11} , (b) % error in L .

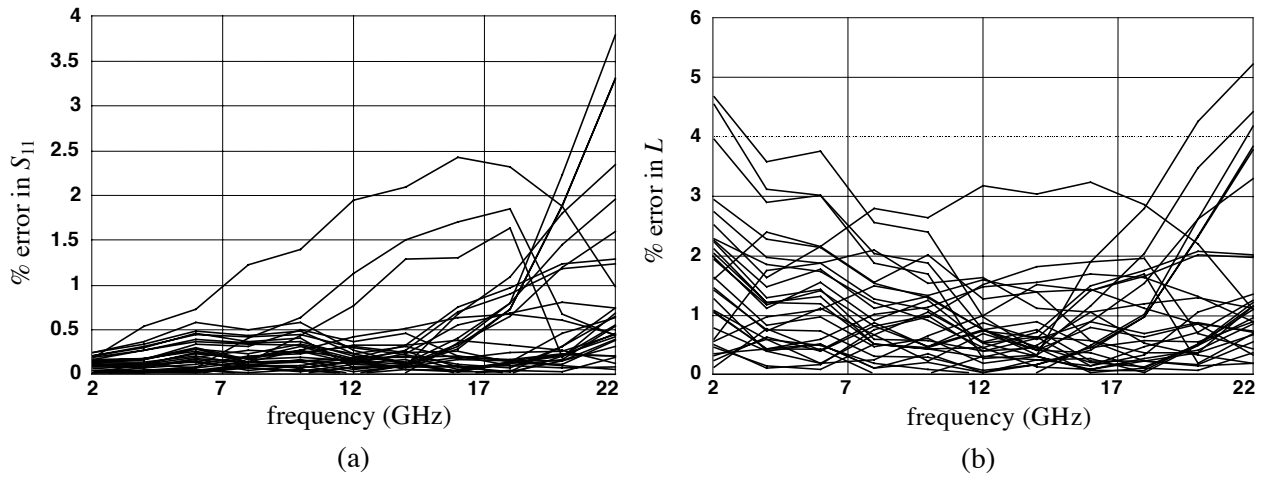


Fig. 16. Comparison of the FDEM of the microstrip via with respect to em^{TM} over a broad frequency range at the test points: (a) % error in S_{11} , (b) % error in L .

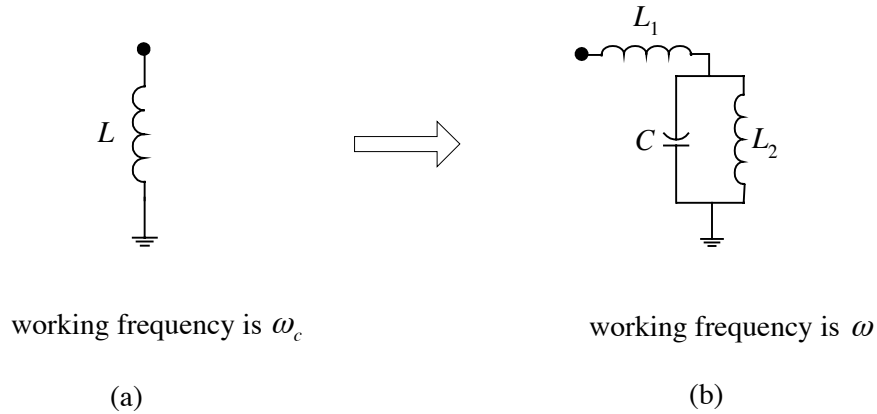


Fig. 17. The FDEM of the microstrip via (a) and the corresponding FIEM (b).

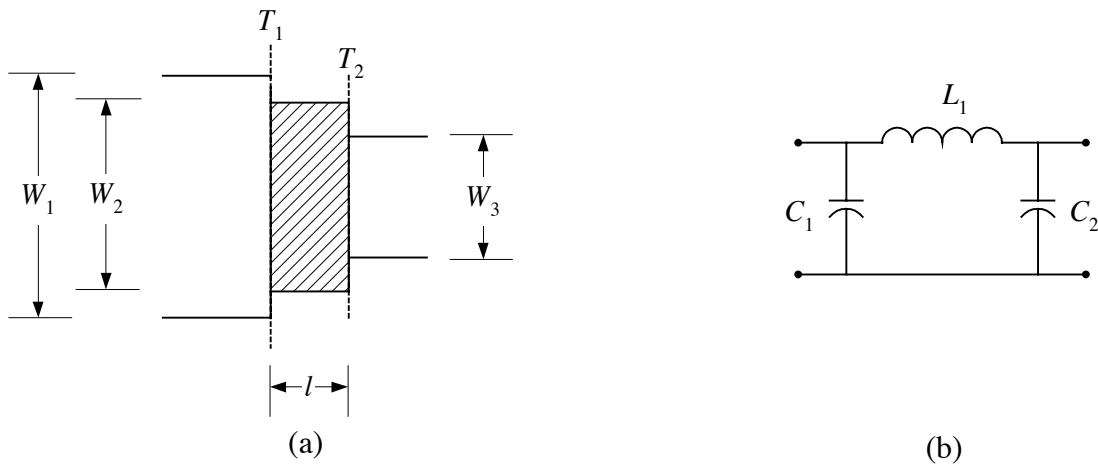


Fig. 18. The microstrip double-step: (a) the physical structure where T_1 and T_2 are the reference planes, (b) the coarse model.

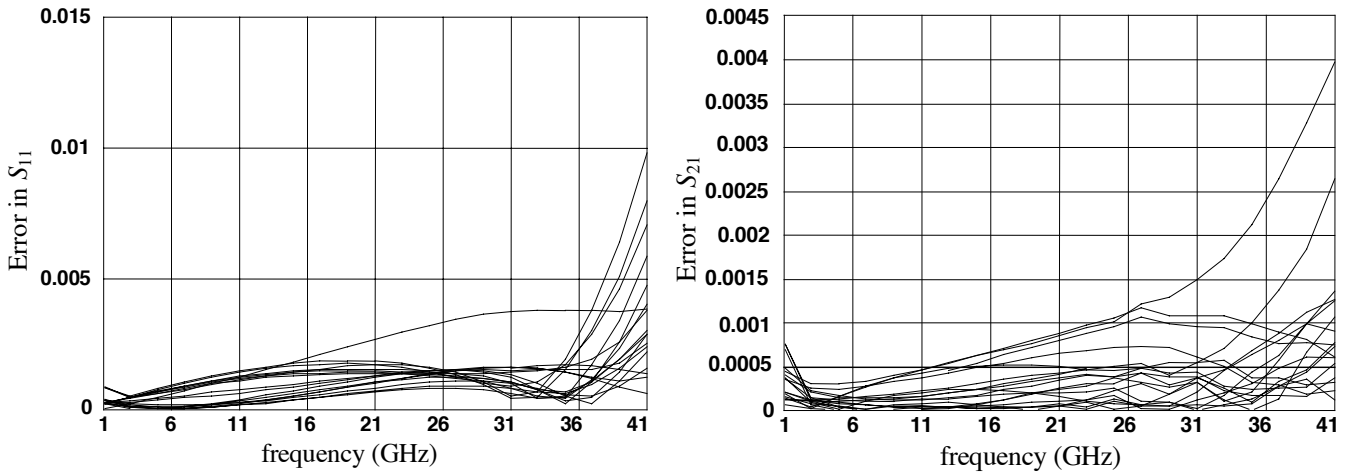


Fig. 19. Comparison between the FDEM of the double-step element and em^{TM} at the test points in the region of interest: (a) error in S_{11} , (b) error in S_{21} .

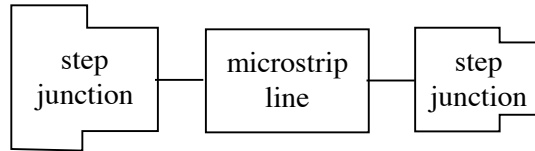


Fig. 20. An alternative model for the microstrip double-step element.

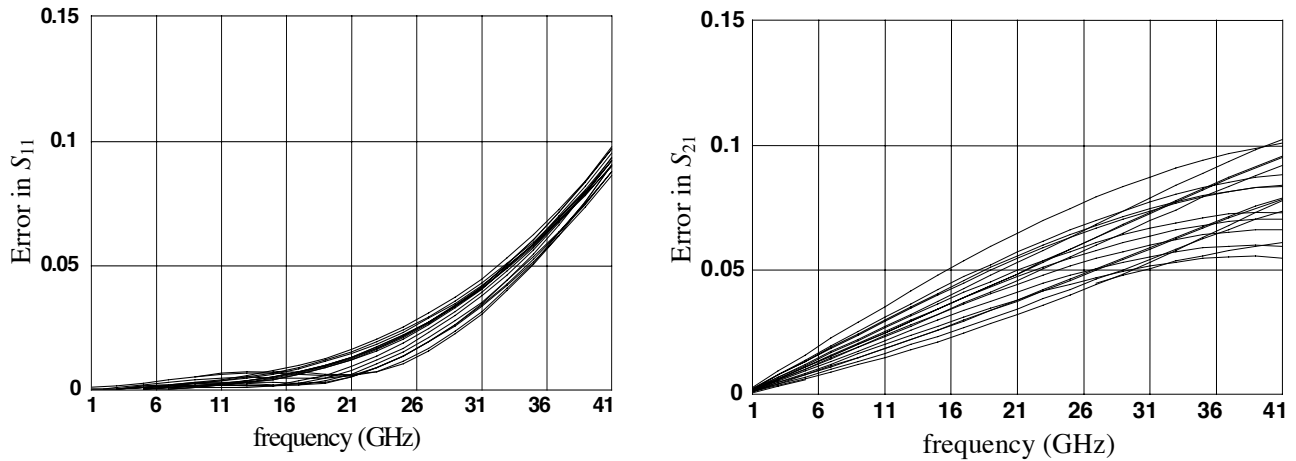


Fig. 21. Comparison between the double-step model in Fig.20 and em^{TM} at the test points in the region of interest: (a) error in S_{11} , (b) error in S_{21} .

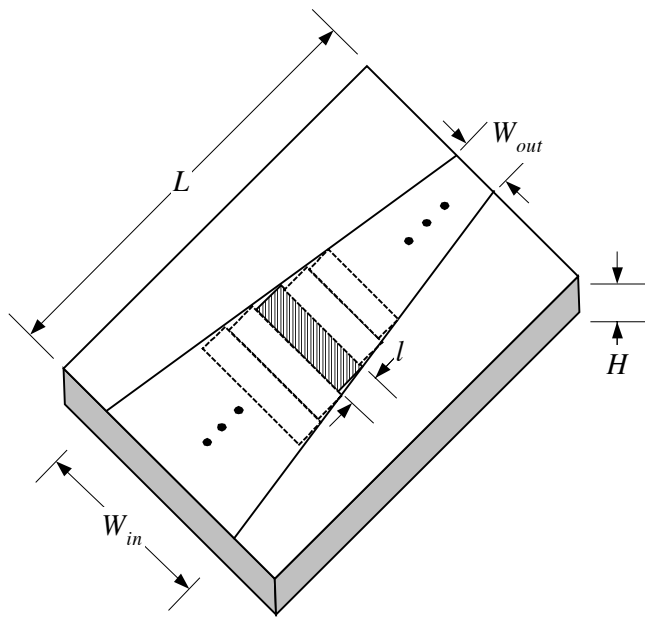


Fig. 22. Linear tapered microstrip line.

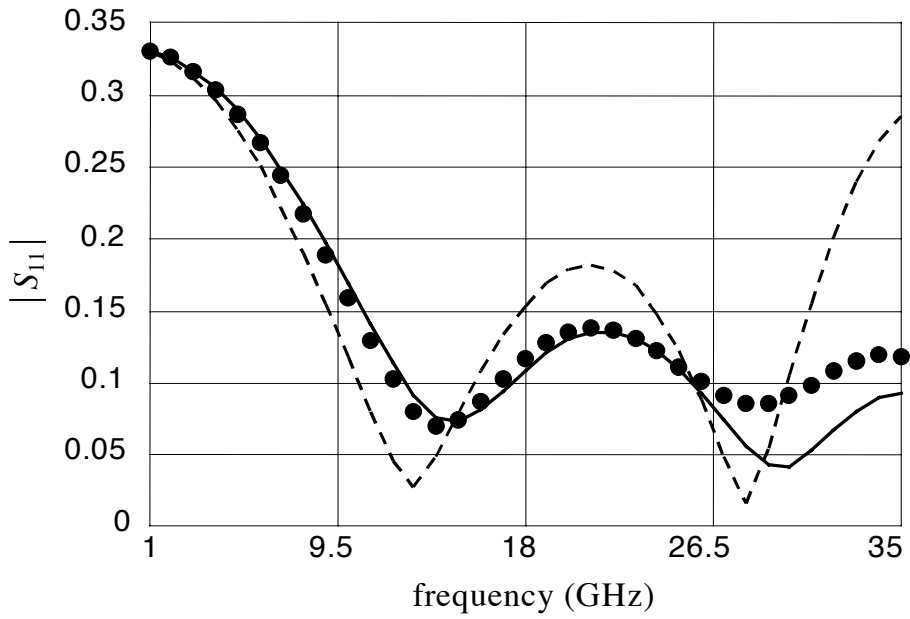


Fig. 23. The response of the linear tapered microstrip line by em^{TM} ($\bullet \bullet$), by the FDEM of the double-step element (—), by the model in Fig.20 of the double-step element (----).

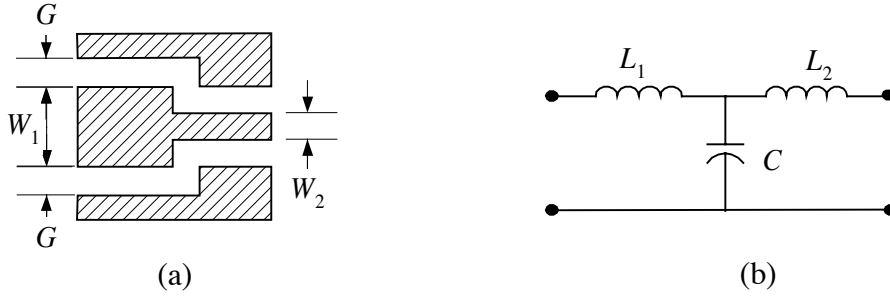


Fig. 24. The CPW step junction: (a) the physical structure, (b) the coarse model.

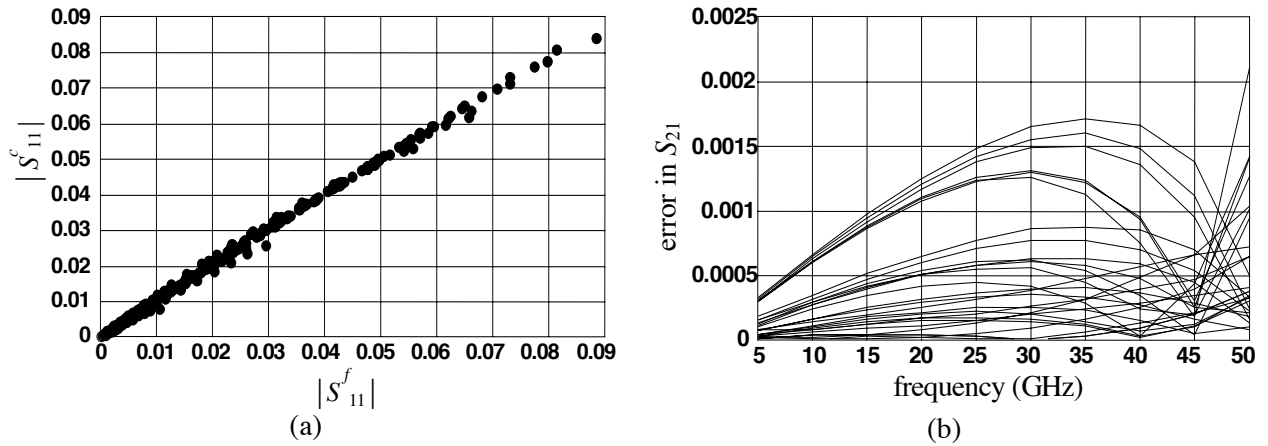


Fig. 25. Comparison between the results obtained by em^{TM} and by the FIEM of the CPW step junction: (a) $|S_{11}|$ by em^{TM} versus that of the FIEM, (b) the error in S_{21} .

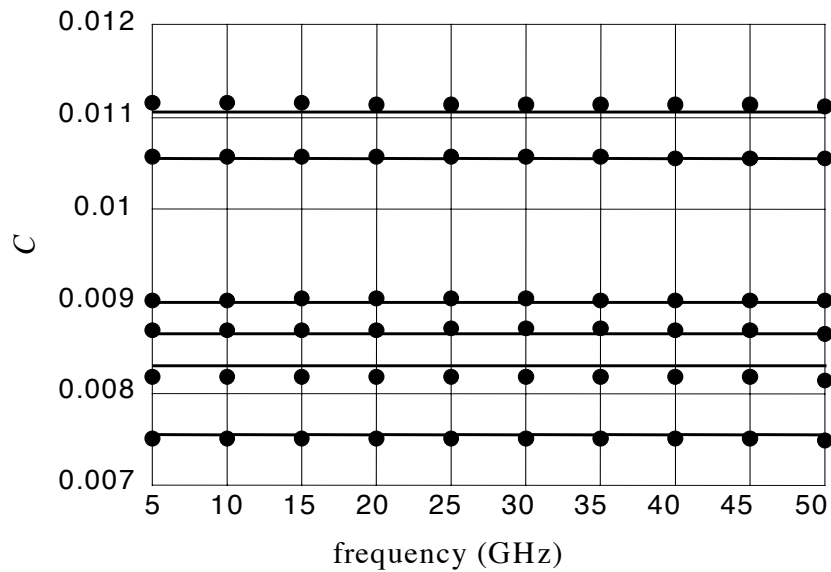


Fig. 26. The capacitance of the CPW step junction: (a) extracted from the fine model ($\bullet \bullet$), (b) predicted by the FIEM of the CPW step junction (---).